New Journal of Physics
The open access journal at the forefront of physics

Deutsche Physikalische Gesellschaft DPG IOP Institute of Physics

PAPER • OPEN ACCESS

Giant spin-orbit torque and spin current generation in carriers at oxide interfaces

To cite this article: Ning Zhang *et al* 2016 *New J. Phys.* **18** 093034

View the article online for updates and enhancements.

You may also like

- Gutzwiller density functional theory: a formal derivation and application to ferromagnetic nickel
Tobias Schickling, Jörg Bünemann, Florian Gebhard et al.
- Designing spin-textured flat bands in twisted graphene multilayers via helimagnet encapsulation
Guangze Chen, Maryam Khosravian, Jose L Lado et al.
- Pressure-induced superconductivity in CrAs and MnP
Jinguang Cheng and Jianlin Luo

This content was downloaded from IP address 141.48.67.87 on 23/12/2024 at 08:16

New Journal of Physics
The open access journal at the forefront of physics

Deutsche Physikalische Gesellschaft DPG
IOP Institute of Physics

Published in partnership with: Deutsche Physikalische Gesellschaft and the Institute of Physics

OPEN ACCESS

RECEIVED
27 April 2016

REVISED
24 August 2016

ACCEPTED FOR PUBLICATION
5 September 2016

PUBLISHED
20 September 2016

Original content from this work may be used under the terms of the Creative Commons Attribution 3.0 licence.

Any further distribution of this work must maintain attribution to the author(s) and the title of the work, journal citation and DOI.

PAPER

Giant spin-orbit torque and spin current generation in carriers at oxide interfaces

Ning Zhang[1], **Yan Wang**[1], **Jamal Berakdar**[2] **and Chenglong Jia**[1,3]

[1] Key Laboratory for Magnetism and Magnetic Materials of MOE, Lanzhou University, Lanzhou 730000, People's Republic of China
[2] Institut für Physik, Martin-Luther Universität Halle-Wittenberg, D-06099 Halle, Germany
[3] Author to whom any correspondence should be addressed.

E-mail: jamal.berakdar@physik.uni-halle.de **and** cljia@lzu.edu.cn

Keywords: spin-orbit effects, oxide interfaces, helimagnet, 2DEG

Abstract

Interfacing polar insulating oxides may result in the formation of interface-confined, high density carriers with a number of emergent properties. A local coupling of carriers to a helimagnetic oxide layer is shown to lead to an effective spin-orbit interaction with a band splitting determined by the local s-d exchange interaction. As a result a bias-induced, non-equilibrium long-lived spin density normal to the spiral plane is predicted. We find that the spin accumulation is strongly enhanced when only one of the two bands is at the Fermi level and the chemical potential is close to the band edge. As a consequence we predict a large spin-transfer torque and spin current emission that can be utilized for oxide-based spintronic applications.

Introduction

Non-magnetic control of spins is essential for a number of spintronic devices with novel functionalities and low-energy consumptions. The driving mechanisms are diverse [1, 2], such as the spin-Hall effect [3–5], current-induced spin torques [6, 7], the spin-Seebeck effect [8], or the magnetoelectric effect [9–13]. Generally, a key common element is the presence of a spin orbital interaction (SOI) which can lead to a substantial current-driven torque or spin accumulation. This in turn can be utilized to steer the magnetization of a ferromagnetic (FM) layer [7] for example. The largest efficiency of spin-transfer torques so far is observed in the topological insulator (TI) bismuth selenide (Bi_2Se_3) with the Rashba SOI [14, 15] and magnetically doped TI hetrostructures [16]. Here we show that the spin-torque ratio (i.e., the strength of the torque per unit charge density) can be further enhanced by orders of magnitude when utilizing an emergent *spin-polarization* of a high-density two-dimensional electron gas (2DEG) or liquid formed at the interface of oxide heterostructures that involve helical magnetic order.

Such 2DEGs with carrier density $\sim 10^{14}$ cm^{-2} and mobility $\sim 10^4$ cm^2 V^{-1} s^{-1} were realized for $LaAlO_3$/$SrTiO_3$ (LAO/STO) or $RTiO_3$/STO *polar* interfaces (where R is a trivalent rare Earth ion) [17]. Moreover, the STO-layer retains the bulk character even down to a thickness of 2 unit cells [18]. This sheet of 2DEG can be excellently confined in STO/1-monolayer-RO/STO heterostructures [19] and STO/$SrTi_{0.8}Nb_{0.2}O_3$ quantum-well structures when the thickness of the $SrTi_{0.8}Nb_{0.2}O_3$ layer becomes less than 1.56 nm [20]. Experiments on the gate-control of the Rashba-type spin–orbit coupling in LAO/STO heterostructures have been reported [21, 22]. Furthermore, experiments [23] evidenced anisotropic magnetoresistance in (STO) quantum wells (<1 nm, with carrier density 7×10^{14} cm^{-2}) epitaxially embedded in ferrimagnetic $GdTiO_3$ (GTO) or antiferromagnetic $SmTiO_3$. What happens if a helimagnet film is involved, e.g. if $RMnO_3$ (R = Tb, Dy, Gd) [24, 25] replaces one of the GTO layer or is deposited atop of highly confined STO quantum wells [20, 26]. Experimentally, the helical spin structure of $TbMnO_3$ (TMO), for instance, is found to persist down to 6nm films on $YAlO_3$ [001] substrates [27]. In this case, due to electronic correlations the 2DEG carriers couple to the local magnetic moments whose spiral structure leads to an (gauge) effective SOI [28]. Acting on traversing carriers this SOI results in an emergent spin polarization of 2DEG, as shown below. Remarkably this effective SOI resembles the semiconductor case for which the Rashba SOI and Dresselhaus SOI have equal strengths

© 2016 IOP Publishing Ltd and Deutsche Physikalische Gesellschaft

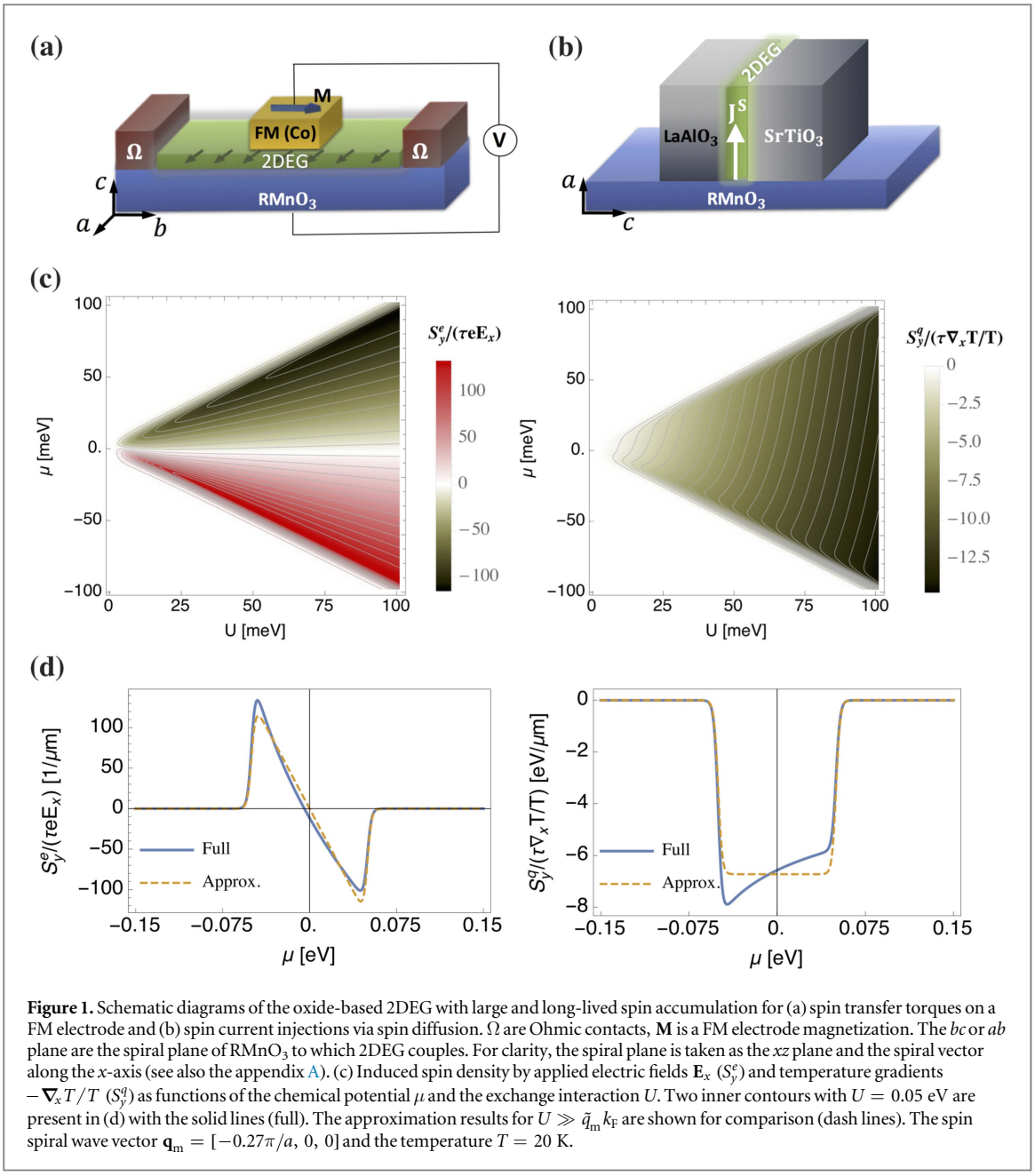

Figure 1. Schematic diagrams of the oxide-based 2DEG with large and long-lived spin accumulation for (a) spin transfer torques on a FM electrode and (b) spin current injections via spin diffusion. Ω are Ohmic contacts, **M** is a FM electrode magnetization. The *bc* or *ab* plane are the spiral plane of $RMnO_3$ to which 2DEG couples. For clarity, the spiral plane is taken as the *xz* plane and the spiral vector along the *x*-axis (see also the appendix A). (c) Induced spin density by applied electric fields $\mathbf{E}_x$ (S_y^e) and temperature gradients $-\boldsymbol{\nabla}_x T/T$ (S_y^q) as functions of the chemical potential μ and the exchange interaction U. Two inner contours with $U = 0.05$ eV are present in (d) with the solid lines (full). The approximation results for $U \gg \tilde{q}_m k_F$ are shown for comparison (dash lines). The spin spiral wave vector $\mathbf{q}_m = [-0.27\pi/a,\ 0,\ 0]$ and the temperature $T = 20$ K.

[29, 30]. Therefore, only a weak decay of spin polarization coherence occurs during a (nonmagnetic) momentum-dependent intra-band scattering. At low temperatures, the inter-band scattering is suppressed because of the band separation stemming from the local s-d exchange interaction. Thus, a large and long-lived spin accumulation emerges in 2DEG as only the lower subband is occupied with electrons. Such a generated spin accumulation is very useful for oxide-based spintronics, e.g., as highly efficient generators of spin transfer torque steering the magnetization of an attached FM layer (see figure 1(a)), or for coherent spin-current injection (see figure 1(b)). Further functionalities are expected with the $RMnO_3$ thin films grown on $YAlO_3$ [27] or STO [31] substrates. For example, some helimagnets (TMO) possess spin-current driven ferroelectric polarization and hence the SOI can be tuned by a moderate electric field [32].

Generalities and proposed setup

The proposed structures are sketched in figures 1(a)–(b). The essential building block is composed of the oxide-based 2DEG and a helimagnet such as TMO (e.g. GTO/STO/TMO or STO/LAO/TMO). Below $T_C = 27$ K, TMO exhibits a spin-driven multiferroicity and a helical spin structure in the *bc* (or *ab*) plane [24, 32]. In the following *xz*-plane is taken as the spiral plane, i.e., $\mathbf{m}(\mathbf{r}) = [\sin \mathbf{q}_m \cdot \mathbf{r},\ 0,\ \cos \mathbf{q}_m \cdot \mathbf{r}]$ with the spiral vector

$\mathbf{q}_m = [-q_m, 0, 0]$. The coupling of 2DEG to the helical spin order is captured by the s-d Hamiltonian

$$H = \frac{\mathbf{P}^2}{2m} + U\boldsymbol{\sigma} \cdot \mathbf{m}(\mathbf{r}). \tag{1}$$

It should be noted that the vector potential associated with the internal (real) magnetic field of the magnetic moments is negligible [28]. $\mathbf{P} = \hbar\mathbf{k}$ is the momentum operator, m is the effective electron mass, U is the local exchange coupling strength, and $\boldsymbol{\sigma}$ is a vector with Pauli matrices components. Performing the unitary local transformation $U_g = \exp(-\mathrm{i}\mathbf{q}_m \cdot \mathbf{r}\sigma_y/2)$, the quantization axis becomes oriented along the vector $\mathbf{m}(\mathbf{r})$ at each point (σ_y does not change, as $[U_g, \sigma_y] = 0$). H then transforms to (a brief summary of mathematical details is included in the appendix A)

$$\tilde{H} = \frac{\hbar^2\mathbf{k}^2}{2m} + \alpha k_x\sigma_y + U\sigma_z \tag{2}$$

with $\alpha = \hbar^2 q_m/(2m)$. Clearly, the transformed Hamiltonian $\tilde{H}$ contains an (gauge) effective SOI that depends linearly on the carriers wave vector $\mathbf{k}$ and on the helicity $\mathbf{q}_m$ of magnetic order. The strength of effective SOI, α is determined by the effective mass m of the 2DEG as well. For the collinear magnetic phase ($\mathbf{q}_m = 0$) this SOI vanishes. Diagonalizing $\tilde{H}$ yields two carrier subbands $E_k^{\pm}$ well-separated by U, i.e.

$$E_k^{\pm} = \varepsilon_k \pm \sqrt{U^2 + \alpha^2 k_x^2} \tag{3}$$

with $\varepsilon_k = \hbar^2\mathbf{k}^2/(2m)$. Note, this band splitting suppresses efficiently the inter-subband scattering at low temperatures. If $U = 0$, the 2DEG decouples completely from the helical magnetic structure and becomes a 2DEG without gauge spin–orbit coupling. We have then $E_k^- = E_k^+$ and effects based on lifting this degeneracy disappear. In our case with given finite U the spiral structure selects a specific value for $\mathbf{q}_m$ resulting in $E_k^- \neq E_k^+$ and associated effects.

For 2DEG at oxide interfaces the effective electron mass $m = 3m_e$ [21, 33, 34] (m_e is the bare electron mass), and $q_m = 0.27\pi/a$ (for TMO [32], a lattice constant $a = 5$ Å is assumed). The effective SOI strength reads then $\alpha = 0.216$ eV Å, which is of the same order as the Rashba SOI in typical semiconductor quantum wells [35, 36]. The $\mathbf{k}$-dependence of the effective SOI is analogous to the Dresselhaus [110] model and the balanced Rashba and Dresselhaus spin–orbit couplings [29, 30, 37, 38], in which case the system possesses an exact SU(2) symmetry that renders spin lifetime infinite. In our case, given the large electron density and the high mobility of oxide electron gases [17], the electron–phonon and electron-impurity scattering are usually weak. Scattering is dominated by Coulomb interactions. However, due to the relatively large Fermi energy (~0.5 eV), a moderate exchange interaction U implies long-lived spin coherence in 2DEG with inhomogeneous direction of spin polarization [39]. Furthermore, the degeneracy of each subband may result in screening of the Coulomb interaction at charged defects [40]. Together with the suppression of the kinetic energy due to the large effective mass, we expect in general large spin-orbit effects in oxide heterostructures.

Induced spin density

By mixing orbital and spin degrees of freedom, the effective SOI suggests a current-induced spin density in 2DEG [7]. Generally, such a non-equilibrium spin density influenced by applied electric fields and temperature gradients can be written as [41]

$$S_i(\omega) = S_i^e(\omega) + S_i^q(\omega) = \kappa_{ij}^{se}(\omega)E_j - \kappa_{ij}^{sq}(\omega)\frac{\nabla_j T}{T}, \tag{4}$$

where i and $j = (x,\ y,$ and $z)$ are spatial subscripts. s, q, and e denote respectively the spin, heat, and charge degrees of freedom. Formally, the conductivities $\kappa_{ij}^{s\nu}$ (here $\nu = e$ or q) is introducible via the linear response function of the homogeneous spin density S_i to a weak vector potential A_j^{ν}. Given that the vector potential A_j^{ν} is related linearly to a current density J_j^{ν}, the response can be denoted by the Kubo product $\ll \hat{S}_i; \hat{J}_j^{\nu} \gg_{\omega}$ [42]. Taking that $\mathbf{A}^e = \mathbf{E}\mathrm{e}^{-\mathrm{i}\omega t}/\mathrm{i}\omega$ and $\mathbf{A}^q = -(\boldsymbol{\nabla}T/T)\mathrm{e}^{-\mathrm{i}\omega t}/\mathrm{i}\omega$, we have [41, 43]

$$\kappa_{ij}^{s\nu} = -\frac{\mathrm{i}T}{\omega}\mathrm{Tr}\int\frac{\mathrm{d}^2\mathbf{k}}{(2\pi)^2}\sum_{\varepsilon_n}\hat{\sigma}_i G_k(\varepsilon_n + \omega)\hat{J}_j^{\nu} G_k(\varepsilon_n), \tag{5}$$

where the charge and heat current densities are

$$\hat{\mathbf{j}}^e = e\hat{\mathbf{v}} \quad \text{and} \quad \hat{\mathbf{j}}^q = \frac{1}{2}[\tilde{H} - \mu, \hat{\mathbf{v}}]_+ \tag{6}$$

with the 'velocity' operator $\hat{\mathbf{v}} = \delta\tilde{H}/\delta\mathbf{P}$. μ is the chemical potential of the system. $G_k(\varepsilon_n)$ is the Matsubara Green function corresponding to the Hamiltonian $\tilde{H}$

$$G_k(\varepsilon_n) = \frac{\varepsilon_n - \varepsilon_k + \mu + U\sigma_z + \alpha k_x \sigma_y}{(\varepsilon_n - E_k^+ + \mu)(\varepsilon_n - E_k^- + \mu)} \tag{7}$$

with $\varepsilon_n = \mathrm{i}(2n+1)\pi T$ for $n \in Z$. The dc conductivity is $\lim_{\omega\to 0}\kappa_{ij}^{s\nu}(\omega)$. From equation (5) follows that only the conductivities $\kappa_{yx}^{s\nu}$ are finite. This means a steady non-equilibrium spin density S_y (normal to the spiral plane) is generated by a steady current J_x^ν in response to electric field E_x and/or temperature gradient $-\nabla_x T/T$ along the spiral wave vector, similar to the Aronov–Lyanda–Geller–Edelstein (ALGE) effect (also known as the Edelstein effect) [44–46]. No spin-Hall conductivity are expected due to our special form of SOI as a result of the coplanar spiral magnetic ordering [28, 41]. Furthermore, we consider (the experimentally relevant) situation where the applied perturbations E_x and $-\nabla_x T/T$ are small such that a linear response approach is viable. Thus, the effect of the induced current J_x^ν on the local magnetic moments is weak and can be neglected. Performing a Matsubara sum over ε_n and for $\omega \to 0$ the static spin density reads

$$\begin{aligned} S_y^e &= -eE_x\alpha \int \frac{k\mathrm{d}k\mathrm{d}\theta}{(2\pi)^2}\tau_k\Bigg[\frac{2\varepsilon_k \sin^2\theta}{\sqrt{U^2+\alpha^2k^2\sin^2\theta}}(n_{\mathrm{F}}'(E_k^+-\mu) - n_{\mathrm{F}}'(E_k^--\mu)) \\ &\quad + (n_{\mathrm{F}}'(E_k^+-\mu) + n_{\mathrm{F}}'(E_k^--\mu))\Bigg], \end{aligned} \tag{8}$$

$$\begin{aligned} S_y^q &= \frac{\nabla_x T}{T}\alpha \int \frac{k\mathrm{d}k\mathrm{d}\theta}{(2\pi)^2}\tau_k\Bigg[\frac{2\varepsilon_k\left(\varepsilon_k - \mu + \frac{m\alpha^2}{\hbar^2}\right)\sin^2\theta}{\sqrt{U^2+\alpha^2k^2\sin^2\theta}}(n_{\mathrm{F}}'(E_k^+-\mu) - n_{\mathrm{F}}'(E_k^--\mu)) \\ &\quad + (\varepsilon_k - \mu + 2\varepsilon_k\,\sin^2\theta)(n_{\mathrm{F}}'(E_k^+-\mu) + n_{\mathrm{F}}'(E_k^--\mu))\Bigg], \end{aligned} \tag{9}$$

where $n_{\mathrm{F}}(\varepsilon)$ (n_{F}') is the Fermi distribution function (its energy derivative). τ_k is the momentum-relaxation time. Obviously the induced spin density vanishes for a collinear spin order in which case $\alpha = 0$. In the limit of $U = 0$, the velocity $\hat{\mathbf{v}}$ and the current density J_j^ν come to be spin-independent and we have $\kappa_{ij}^{s\nu} = 0$, leading to a vanishing spin density as well. For strong s-d exchange interaction $U \gg \alpha k_{\mathrm{F}}$ with k_{F} being the Fermi wave vector, the above equations evidence a linear q_{m}-dependence of S_y (see the dash lines in figure 2). The sign of q_{m} and hence of S_y is invertible by a transverse E field.

For low temperature $n_{\mathrm{F}}'(\varepsilon)$ is strongly peaked which yields

(i) For $\mu < -U$ or $\mu > U$, both subbands are then occupied by electrons or holes, respectively. We have vanishing spin density

$$S_y^e \approx 0 \text{ and } S_y^q \approx 0. \tag{10}$$

(ii) For $|\mu| < U$, only the lower subband, E_k^- is electronically populated. From equations (8)–(9) one finds

$$S_y^e = -\frac{q_{\mathrm{m}}}{4\pi}\tau_{k_{\mathrm{F}}} eE_x \frac{\mu}{U} \text{ and } S_y^q = -\frac{q_{\mathrm{m}}}{4\pi}\tau_{k_{\mathrm{F}}}\frac{\nabla_x T}{T}U, \tag{11}$$

where $\tau_{k_{\mathrm{F}}}$ is the relaxation time at the Fermi wave vector.

Equations (10) and (11) are the main analytical results. Assuming that the spiral wave vector $q_{\mathrm{m}} = 0.27\pi/a$, $U \sim 10$ meV, and $|\mu/U| \sim 1$, in the case of only E_k^- being occupied we have $S_y^e/(\tau_{k_{\mathrm{F}}} eE_x) \sim 10^2\ \mu\mathrm{m}^{-1}$ and $S_y^q/(\tau_{k_{\mathrm{F}}}\nabla_x T/T) \sim 10^3$ meV $\mu\mathrm{m}^{-1}$, which are two orders larger than the values of GaAs-based quantum wells with the Rashba SOI in [43]. In figure 1, numerical results of spin density, given by equations (8) and (9) with or without the approximation $U \gg \alpha k_{\mathrm{F}}$, are shown as functions of μ and U and $T = 20$ K which is below the multiferroic transition temperature of TMO [24, 32]. The low-temperature approximate solutions, equations (10) and (11) explain well the spin polarization behavior. The spin density is strongly enhanced only if the lower subband (E_k^-) is occupied with electrons as $|\mu| < U$ (see figure 1(d)) and achieves its extremal value at the band edge. The small discrepancies stem from deviation from $U \gg \alpha k_{\mathrm{F}}$ when SOI coefficient α is large (see figure 2). Here we emphasize that this spin density survives even for weak s-d exchange interaction as long as the thermal excitation energy is lower than the band splitting (i.e., $kT \ll U$) and $\mu/U \approx 1$. For $|\mu| > U$ both subbands are occupied with electrons or nearly empty. The numerical results show a non-zero spin density (see figure 2), which is two orders of magnitude lower than the values with only the E_k^- being occupied, however it is still the same amplitudes as that in semiconductor quantum wells with Rashba SOI [43]. Whereas, the linear q_{m}-dependence of the spin polarization S_y^ν holds for all cases with weak effective SOI. Experimentally, such large and long-lived spin density at complex oxide interfaces is advantageous for highly efficient spin-orbit effects, as discussed below.

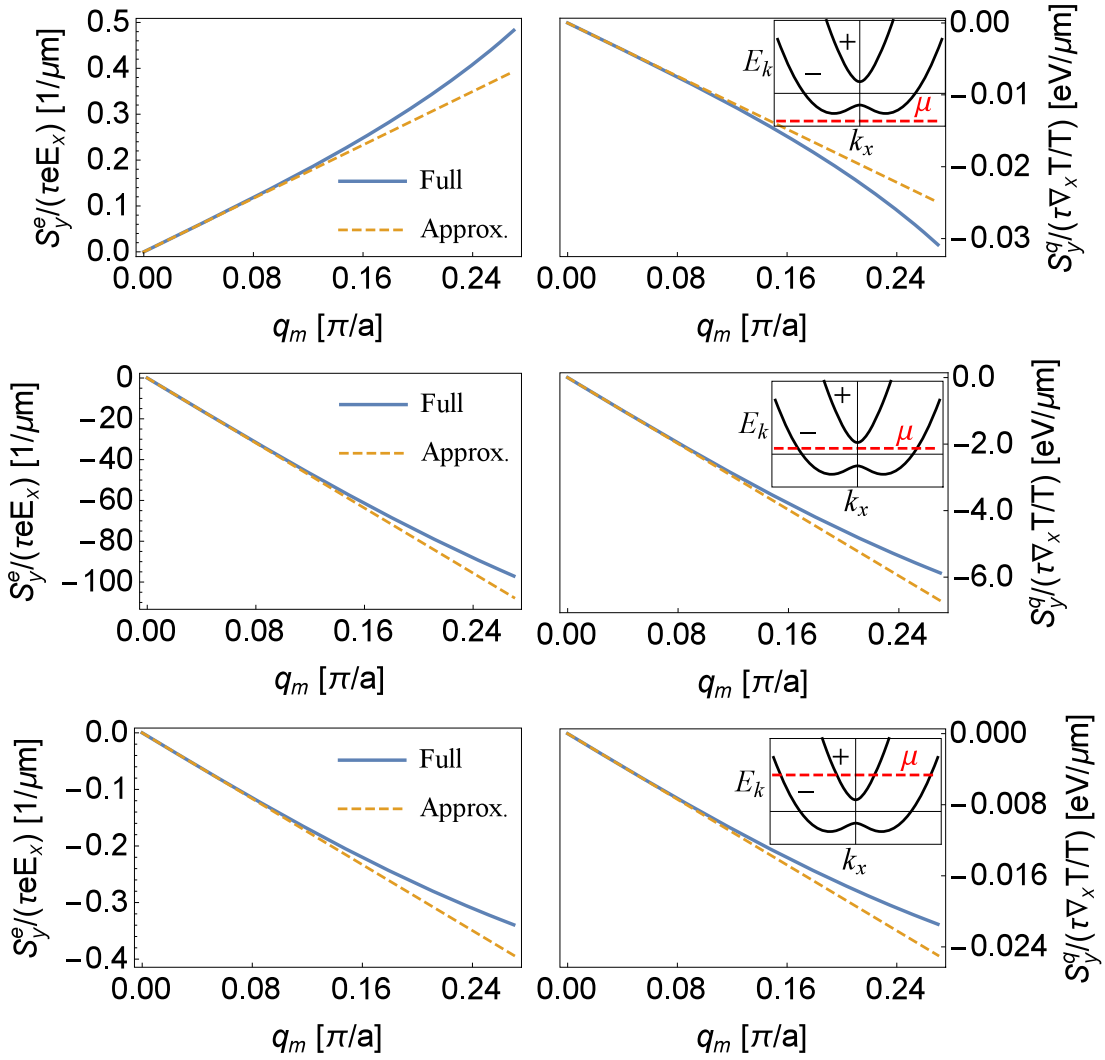

Figure 2. The q_m-dependence of the spin density with $U = 0.05$ eV for various values of the chemical potential (see the insets): $\mu = -0.06$ eV in the first row, $\mu = 0.04$ eV in the second row, and $\mu = 0.06$ eV in the third row, respectively.

Giant spin transfer torques

Different from the usual case of a pure Hall-effect geometry, in which a spin toque would be due to a spin current injected into a FM layer, here the diffusion of the spin accumulation from the 2DEG results in a giant spin transfer torques, e.g., on a FM top electrode, for instance, a Co electrode (see figure 1(a) and [47]). Let the thickness of the FM layer be $d_{\rm FM}$ and the z axis has its origin at the 2DEG/FM interface. In the steady-state regime the boundary conditions of itinerant spin density, $\mathbf{S}_{\rm FM}(z)$ in the FM are [14]: $\mathbf{S}_{\rm FM}(0) = \mathbf{S}_0$ and $\mathcal{J}^{\rm s}_{\rm FM}(d_{\rm FM}) = 0$, where the spin current $\mathcal{J}^{\rm s}_{\rm FM}(z) = -\mathcal{D}_0\nabla_z\mathbf{S}_{\rm FM}(z)$ with $\mathcal{D}_0$ being the diffusion coefficient. From the equations governing the spin dynamics in the FM layer [48], the diffusion leads to a steady-state (itinerant) spin distribution [14]

$$\mathbf{S}_{\rm FM}(z) = S_{\parallel}(z) + \mathrm{i}S_{\perp}(z) = S_0\frac{\cosh[(z - d_{\rm FM})/\lambda_{\rm m}]}{\cosh(d_{\rm FM}/\lambda_{\rm m})}, \tag{12}$$

where $\lambda_{\rm m} = \sqrt{\mathcal{D}_0/(\tau_{\rm sf}^{-1} + \tau_\phi^{-1} - i\tau_J^{-1})}$ with τ_J, τ_ϕ, and $\tau_{\rm sf}$ being the spin precession time, the spin decoherence time, and the spin diffusion-time in the FM electrode, respectively. $\mathbf{S}_{\rm FM}$ is perpendicular to the FM magnetization. The initial (three-dimensional) spin density $\mathbf{S}_0$ is assumed to be aligned with the spin accumulation in 2DEG due to the exchange interaction, $\mathbf{S}_0 = \chi\mathbf{S}''/d_{\rm EG}$ where $d_{\rm EG}$ is the thickness of the electron gas. χ describes the interface effect and is of the order 1 [14]. The spin torque on the FM moments is defined as the spatial change of the spin current compensated by the spin relaxation [14, 48]

$$\mathbf{T} = \int_0^{d_{\rm FM}} \mathrm{d}z \left[-\boldsymbol{\nabla} \cdot \boldsymbol{\mathcal{J}}^{\rm s}_{\rm FM}(z) - \frac{1}{\tau_{sf}} \mathbf{S}_{\rm FM}(z) \right]. \tag{13}$$

In the limit of a thick FM layer, we find $\mathbf{T} = S_0 \lambda_{\rm m} (\tau_\phi^{-1} - \mathrm{i}\tau_J^{-1})$. The spin torque ratio is defined as, $\boldsymbol{\theta}_{\rm ST} = \mathbf{2eT}/(\hbar J_x^e)$. For spin accumulation induced by the applied electric field E_x we have then

$$\boldsymbol{\theta}_{\rm ST} = \chi \frac{2e}{\hbar} \frac{S_y^e}{\kappa_x^e E_x} \frac{\lambda_{\rm m}}{d_{\rm EG}} (\tau_\phi^{-1} - \mathrm{i}\tau_J^{-1}). \tag{14}$$

The charge current density is $J_x^e = \kappa_x^e E_x$ where κ_x^e is the charge conductivity of 2DEG. Introducing the spin density S_y^e, equation (11) into the spin torque ratio, one finds

$$\boldsymbol{\theta}_{\rm ST} = -\chi \frac{\sigma_0}{\kappa_x^e d_{\rm EG}} \frac{q_{\rm m} \lambda_{\rm m}}{2} \frac{\mu}{U} \left(\frac{\tau_{k_{\rm F}}}{\tau_\phi} - \mathrm{i} \frac{\tau_{k_{\rm F}}}{\tau_J} \right). \tag{15}$$

$\sigma_0 = 2e^2/h$ is the conductance quantum. Using the effective electrical conductivity of STO/$SrTi_{0.8}Nb_{0.2}O_3$ quantum well, $\kappa_x^e = 1.4 \times 10^2$ S cm^{-1} [20], together with $d_{\rm EG} = 5$ nm, $q_{\rm m} = 0.27\pi/a$ for TMO [32], and $\lambda_{\rm m} = 40$ nm for Co [49], the spin torque ratio is

$$\boldsymbol{\theta}_{\rm ST} \approx -37.6\chi \frac{\mu}{U} \left(\frac{\tau_{k_{\rm F}}}{\tau_\phi} - \mathrm{i} \frac{\tau_{k_{\rm F}}}{\tau_J} \right). \tag{16}$$

For a typical ferromagnet (Ni, Co, Fe and their alloys), $\tau_\phi = \tau_J = 10^{-14}$ s [14, 48, 50]. The average momentum relaxation time $\bar{\tau}_{k_{\rm F}}$ in 2DEG is estimated by $u = e\bar{\tau}_{k_{\rm F}}/m$, where u is the mobility ($\sim 10^4$ cm^2 V^{-1} s^{-1}) of 2DEG at oxide interfaces [17, 51, 52]. We have then $\bar{\tau}_{k_{\rm F}} = 10^{-11} - 10^{-12}$ s as observed in experiments [21, 33], which results in a giant spin torque ratio, $|\boldsymbol{\theta}_{\rm ST}| \sim 10^3 - 10^4$, at the band edge ($|\mu/U| \approx 1$), compared to the value ($\sim$2.0–3.5) in the TI Bi_2Se_3 [14].

Long-range spin current

Alternatively, considering the spin-current injection geometry as shown in figure 1(b), by vertically depositing the LAO/STO heterostructures on $RMnO_3$ substrates, the diffusion of spin accumulation from the 2DEG/helimagnet interface yields an exponential spin distribution in 2DEG, $\mathbf{S}(z) = \mathbf{S}_0 \mathrm{e}^{-z/\lambda_{\rm EG}}$ and thus a long-lived spin current

$$\mathbf{J}^{\rm s}(z) = \mathbf{S}_0 \mathcal{D}_0 \mathrm{e}^{-z/\lambda_{\rm EG}}/\lambda_{\rm EG}, \tag{17}$$

along the $a(z)$-direction. Here $\lambda_{\rm EG}$ is the spin diffusion length in 2DEG, which is expected beyond μm. Accounting for the Rashba SOI at LAO/STO interfaces, $\alpha_R(k_a\sigma_b - k_b\sigma_a)$ that arises due to a break of the structural inversion symmetry [21, 53], we infer that the spin current $\mathbf{J}^{\rm s}(z)$ leads to a transverse charge current via an inverse ALGE effect [54] or inverse spin-Hall effect [55] depending on the direction of interfacial spin density $\mathbf{S}_0$: *(i)* In-plane $\mathbf{S}_0 \| a$ with the bc spiral, the induced charge current by inverse ALGE effect along the b-axis reads, $J_b^e(z) = \alpha_R \bar{\tau} J_a^{\rm s}(z)$. *(ii)* Out-of-plane $\mathbf{S}_0 \| c$ with the ab being the spiral plane: the transverse charge current induced by the momentum scattering in the Rashba SOI leads here to a charge current along the b direction such that $J_b^e(z) = \gamma \frac{2e}{\hbar} J_c^{\rm s}(z)$, where γ is the inverse spin-Hall angle. In an open circuit geometry, the generated electric field E_b satisfies $\int_0^{h_{\rm EG}} [J_b^e(z) + \kappa_b^e E_b] \mathrm{d}z = 0$, which gives

$$E_b = -\frac{1}{\kappa_b^e h_{\rm EG}} \int_0^{h_{\rm EG}} J_b^e(z) \mathrm{d}z, \tag{18}$$

along the spiral axis. $h_{\rm EG}$ is the thickness of STO heterostructures and κ_b^e is the effective electrical conductivity of 2DEG along the b direction. E_b would lead to a transverse voltage, which can in turn be used for measuring the spin accumulation and other parameters for optimizing the 2DEG/helimagnet building block.

Discussions

Our analysis assumes that the magnetic order is exactly coplanar in the spiral plane but it usually has a small deviation in experiment. This would result in an another (random) weak effective SOI in the spiral plane and introduces a spin dephasing in 2DEG. On the other hand, the parity symmetry breaking at the $RMnO_3$ interfaces due to ferroelectric polarizations in cycloidal $RMnO_3$ gives rise to a conventional Rashba-type SOI. Comparing the saturated polarization in $RMnO_3$ ($\sim 5 \times 10^{-4}$ C m^{-2} [32]) with that in $SrTiO_3$ interfaces ($\sim$0.1C m^{-2} [34]), the strength of the Rashba SOI at the $RMnO_3$ interface is expected to be however much smaller than 10^{-2} eV Å at $SrTiO_3$ interfaces [21], which is already less than 10% of the gauge effective SOI considered here. Therefore, the average spin decoherence induced by these corrections is small. Furthermore, the electric field [32] and

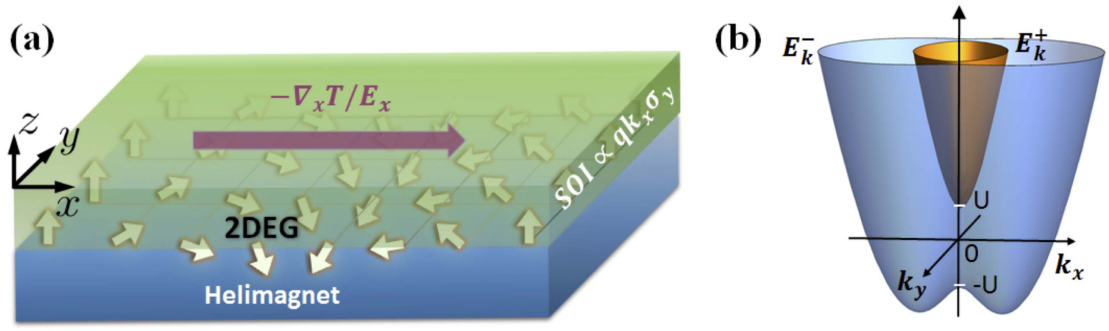

Figure 3. (a) Schematics of the coupled 2DEG/helimagnet heterostructure. The x axis is defined along the direction of the spiral ordering and xz plane as the spiral plane. (b) Energy bands of 2DEG: the band splitting between two energy branches $E_k^{\pm}$ is determined by the local s-d exchange interaction with the strength U.

magnetic field [31] tuning the spiral spin structure (i.e. $q_{\rm m}$) offer new ways to manipulate spin torques. Very recently, extreme mobility enhancement of 2DEG is found at LAO/STO interface by inserting a single-unit-cell insulating layer of $La_{1-x}Sr_xMnO_3$ (LSMO) [56]. Mn^{2+} sites with strong spin–orbit coupling are mostly trapped in the LSMO buffer layer, whereas the 2DEG carriers stay on the Ti site. In principle, the Dzyaloshinskii–Moriya interaction would arise from spin-orbit scattering of electrons in an inversion-asymmetric crystal field [57], we have then helical magnetic order and polar LSMO buffer layer [58], which could be another promising candidate of helimagnetic ultra-thin film in our considerations.

Acknowledgments

This work is supported by NBRPC (No. 2012CB933101), NSFC (No. 11474138), the German Research Foundation (No. SFB 762), and PCSIRT (No. IRT1251). Consultations with Vitalii Dugaev are gratefully acknowledged.

Appendix A. Effective SOI and spinor state of 2DEG

Without loss of generality, let's take the xz-plane as the spiral plane and the spin spiral vector along the x-axis (see figure 3(a)), the local magnetization of the helimagnet reads then

$$\mathbf{m}(\mathbf{r}) = [\sin \mathbf{q}_{\rm m}\cdot\mathbf{r},\ 0,\ \cos \mathbf{q}_{\rm m}\cdot\mathbf{r}], \tag{A.1}$$

where $\mathbf{q}_{\rm m} = [-q_{\rm m},\ 0,\ 0]$ is the spiral vector. At low temperature, the magnetization dynamics is much slower than that of the 2DEG carriers, so we can treat the local magnetic moments as classical and static. By interfacing 2DEG and the helimagnet, the carriers are subject to the local s-d exchange interaction and the dynamics of the 2DEG is governed by the Hamiltonian equation (1). Upon the gauge transformation $U_g(r) = \exp(-{\rm i}\mathbf{q}_{\rm m}\cdot\mathbf{r}\sigma_y/2)$, the quantization axis becomes oriented along the vector $\mathbf{m}(\mathbf{r})$ at each point. It simplifies the last spatially inhomegeneous term in equation (1) as $U_g^{\dagger}(r)[\boldsymbol{\sigma}\cdot\mathbf{m}(\mathbf{r})]U_g(r) = \sigma_z$. Such a transformation introduces however an additional (spinor) gauge potential $\mathbf{A}_g = -{\rm i}\hbar U_g^{\dagger}(r)\nabla_r U_g(r) = -\hbar\sigma_y\mathbf{q}_{\rm m}/2$ as a part of the transformed kinetic energy, i.e., we have the transformed Hamiltonian of the 2DEG

$$\tilde{H} = \frac{1}{2m}(\mathbf{P}+\mathbf{A}_g)^2 + U\sigma_z. \tag{A.2}$$

Gauging away the uniform energy displacement $\Delta E = \mathbf{A}_g^2/2m$, we get then equation (2) and an effective SOI, $\alpha k_x\sigma_y$ with $\alpha = \hbar^2 q_{\rm m}/(2m)$. Clearly, the gauge effective SOI is determined purely by the nontrivial topology of the spiral magnetic texture, and its strength depends linearly on the carriers wave vector $\mathbf{k}$ and on the magnetic spiral helicity $\mathbf{q}_{\rm m}$. For the collinear magnetic phase ($q_{\rm m}\to 0$) this effective SOI vanishes.

By diagonalizing the Hamiltonian $\tilde{H}$, we have two carrier subbands shown in figure 3(b)

$$E_k^{\pm} = \hbar^2(k_x^2+k_y^2)/2m \pm \sqrt{U^2+\alpha^2k_x^2}. \tag{A.3}$$

The corresponding eigenstates are respectively

$$|\psi_+\rangle = e^{i\mathbf{k}\cdot\mathbf{r}}\begin{pmatrix}\cos\frac{\phi}{2}\\ i\ \sin\frac{\phi}{2}\end{pmatrix}, \quad |\psi_-\rangle = e^{i\mathbf{k}\cdot\mathbf{r}}\begin{pmatrix}i\ \sin\frac{\phi}{2}\\ \cos\frac{\phi}{2}\end{pmatrix} \tag{A.4}$$

with $\tan\phi = \frac{\alpha k_x}{U}$.

Noting that σ_y does not change because $[\sigma_y,\ U_g(r)] = 0$, one finds the expectation value of the spin polarization $\langle\sigma_y\rangle$ per electron in the original spin space as

$$\langle\sigma_y\rangle_\pm = \langle\psi_\pm|\sigma_y|\psi_\pm\rangle = \pm\frac{\alpha k_x}{\sqrt{U^2 + \alpha^2 k_x^2}}. \tag{A.5}$$

Obviously, $\langle\sigma_y\rangle$ is odd in k_x, and hence it would vanish upon the summation over a symmetric $\mathbf{k}$ space. However, in the presence of an electric field and/or a temperature gradient along the x direction, the Fermi surface is displaced. We find thus $\langle k_x\rangle \neq 0$ and consequently a finite value of the induced spin density $S_y = \hbar\ \langle\sigma_y\rangle/2$. The other two components, $\langle\sigma_x\rangle$ and $\langle\sigma_z\rangle$ are periodic in the original space and averaged so to zero.

References

[1] Fert A 2008 Nobel lecture: origin, development, and future of spintronics *Rev. Mod. Phys.* **80** 1517–30
[2] Bader S D and Parkin S S P 2010 Spintronics *Annu. Rev. Condens. Matter Phys.* **1** 71–88
[3] Nagaosa N, Sinova J, Onoda S, MacDonald A H and Ong N P 2010 Anomalous Hall effect *Rev. Mod. Phys.* **82** 1539–92
[4] Maciejko J, Hughes T L and Zhang S-C 2011 The quantum spin Hall effect *Annu. Rev. Condens. Matter Phys.* **2** 31–53
[5] Jungwirth T *et al* 2014 Spin-dependent phenomena and device concepts explored in (Ga,Mn)As *Rev. Mod. Phys.* **86** 855–96
[6] Brataas A, Kent A D and Ohno H 2012 Current-induced torques in magnetic materials *Nat. Mater.* **11** 372–81
[7] Brataas A and Hals K M D 2014 Spin-orbit torques in action *Nat. Nanotechnol.* **9** 86–8
[8] Bauer G E W, Saitoh E and van Wees B J 2012 Spin caloritronics *Nat. Mater.* **11** 391–9
[9] Eerenstein W, Mathur N D and Scott J F 2006 Multiferroic and magnetoelectric materials *Nature* **442** 759–65
[10] Bibes M and Barthelemy A 2008 Multiferroics: towards a magnetoelectric memory *Nat. Mater.* **7** 425–6
[11] Martin L W *et al* 2008 Multiferroics and magnetoelectrics: thin films and nanostructures *J. Phys.: Condens. Matter* **20** 434220
[12] Vaz C A F 2012 Electric field control of magnetism in multiferroic heterostructures *J. Phys.: Condens. Matter* **24** 333201
[13] Matsukura F, Tokura Y and Ohno H 2015 Control of magnetism by electric fields *Nat. Nanotechnol.* **10** 209–20
[14] Mellnik A R *et al* 2014 Spin-transfer torque generated by a topological insulator *Nature* **511** 449–51
[15] Wang Y *et al* 2015 Topological surface states originated spin-orbit torques in Bi_2Se_3 *Phys. Rev. Lett.* **114** 257202
[16] Fan Y *et al* 2014 Magnetization switching through giant spin-orbit torque in a magnetically doped topological insulator heterostructure *Nat. Mater.* **13** 699–704
[17] Stemmer S and James Allen S 2014 Two-dimensional electron gases at complex oxide interfaces *Annu. Rev. Mater. Res.* **44** 151–71
[18] Bern F *et al* 2013 Structural, magnetic and electrical properties of $SrRuO_3$ films and $SrRuO_3/SrTiO_3$ superlattices *J. Phys.: Condens. Matter* **25** 496003
[19] Jang H W *et al* 2011 Metallic and insulating oxide interfaces controlled by electronic correlations *Science* **331** 886–9
[20] Ohta H *et al* 2007 Giant thermoelectric Seebeck coefficient of a two-dimensional electron gas in $SrTiO_3$ *Nat. Mater.* **6** 129–34
[21] Caviglia A D *et al* 2010 Tunable rashba spin-orbit interaction at oxide interfaces *Phys. Rev. Lett.* **104** 126803
[22] Hurand S *et al* 2015 Field-effect control of superconductivity and rashba spin–orbit coupling in top-gated $LaAlO_3/SrTiO_3$ devices *Sci. Rep.* **5** 12751
[23] Jackson C A and Stemmer S 2013 Interface-induced magnetism in perovskite quantum wells *Phys. Rev.* B **88** 180403
[24] Kimura T *et al* 2003 Magnetic control of ferroelectric polarization *Nature* **426** 55–8
[25] Tokura Y and Seki S 2009 Multiferroics with spiral spin orders *Adv. Mater.* **22** 1554–65
[26] Tinkl V, Breitschaft M, Richter C and Mannhart J 2012 Large negative electronic compressibility of $LaAlO_3$–$SrTiO_3$ interfaces with ultrathin $LaAlO_3$ layers *Phys. Rev.* B **86** 075116
[27] Glavic A *et al* 2013 Stability of spin-driven ferroelectricity in the thin-film limit: coupling of magnetic and electric order in multiferroic $TbMnO_3$ films *Phys. Rev.* B **88** 054401
[28] Jia C and Berakdar J 2009 Electrically controlled persistent spin currents at the interface of multiferroic oxides *Phys. Rev.* B **80** 014432
[29] Schliemann J, Egues J C and Loss D 2003 Nonballistic spin-field-effect transistor *Phys. Rev. Lett.* **90** 146801
[30] Bernevig B A, Orenstein J and Zhang S-C 2006 Exact su(2) symmetry and persistent spin helix in a spin–orbit coupled system *Phys. Rev. Lett.* **97** 236601
[31] Lu C *et al* 2013 Polarization enhancement and ferroelectric switching enabled by interacting magnetic structures in $DyMnO_3$ thin films *Sci. Rep.* **3** 1–7
[32] Yamasaki Y *et al* 2007 Electric control of spin helicity in a magnetic ferroelectric *Phys. Rev. Lett.* **98** 147204
[33] Ben Shalom M, Ron A, Palevski A and Dagan Y 2010 Shubnikov-de Haas oscillations in $SrTiO_3/LaAlO_3$ interface *Phys. Rev. Lett.* **105** 206401
[34] Copie O *et al* 2009 Towards two-dimensional metallic behavior at $LaAlO_3/SrTiO_3$ interfaces *Phys. Rev. Lett.* **102** 216804
[35] Winkler R, Papadakis S, De Poortere E and Shayegan M 2003 *Spin–Orbit Coupling in Two-Dimensional Electron and Hole Systems* vol 41 (Berlin: Springer)
[36] Ast C R *et al* 2007 Giant spin splitting through surface alloying *Phys. Rev. Lett.* **98** 186807
[37] Tokatly I V and Sherman E Ya 2010 Gauge theory approach for diffusive and precessional spin dynamics in a two-dimensional electron gas *Ann. Phys.* **325** 1104–17
[38] Tokatly I V and Sherman E Ya 2010 Duality of the spin and density dynamics for two-dimensional electrons with a spin–orbit coupling *Phys. Rev.* B **82** 161305(R)
[39] Pershin Y V 2005 Long-lived spin coherence states in semiconductor heterostructures *Phys. Rev.* B **71** 155317

[40] Kamiya T and Kawasaki M 2008 ZnO-based semiconductors as building blocks for active devices *MRS Bull.* **33** 1061–6
[41] Jia C and Berakdar J 2011 Thermoelectric effect of multiferroic oxide interfaces *Appl. Phys. Lett.* **98** 042110
[42] Coleman P 2015 *Introduction to Many-Body Physics* (Cambridge: Cambridge University Press)
[43] Dyrdał A, Inglot M, Dugaev V K and Barnaś J 2013 Thermally induced spin polarization of a two-dimensional electron gas *Phys. Rev.* B **87** 245309
[44] Aronov A G and Lyanda-Geller Yu B 1989 Nuclear electric resonance and orientation of carrier spins by an electric field *JETP Lett.* **50** 431
[45] Edelstein V M 1990 Spin polarization of conduction electrons induced by electric current in two-dimensional asymmetric electron systems *Solid State Commun.* **73** 233–5
[46] Johansson A, Henk J and Mertig I 2016 Theoretical aspects of the edelstein effect for anisotropic two-dimensional electron gas and topological insulators *Phys. Rev.* B **93** 195440
[47] Reyren N *et al* 2012 Gate-controlled spin injection at $LaAlO_3/SrTiO_3$ interfaces *Phys. Rev. Lett.* **108** 186802
[48] Manchon A, Matsumoto R, Jaffres H and Grollier J 2012 Spin transfer torque with spin diffusion in magnetic tunnel junctions *Phys. Rev.* B **86** 060404
[49] Bass J and Pratt W P Jr 2007 Spin-diffusion lengths in metals and alloys, and spin-flipping at metal/metal interfaces: an experimentalist's critical review *J. Phys.: Condens. Matter* **19** 183201
[50] Zhang S and Li Z 2004 Roles of nonequilibrium conduction electrons on the magnetization dynamics of ferromagnets *Phys. Rev. Lett.* **93** 127204
[51] Glazov M M, Sherman E Ya and Dugaev V K 2010 Two-dimensional electron gas with spinšCorbit coupling disorder *Physica* E **42** 2157–77
[52] Bindel J R, Pezzotta M, Ulrich J, Liebmann M, Sherman E Ya and Morgenstern M 2016 Probing variations of the Rashba spin–orbit coupling at the nanometre scale *Nat. Phys.* (doi:10.1038/nphys3774)
[53] Ben Shalom M, Sachs M, Rakhmilevitch D, Palevski A and Dagan Y 2010 Tuning spin–orbit coupling and superconductivity at the $SrTiO_3/LaAlO_3$ interface: a magnetotransport study *Phys. Rev. Lett.* **104** 126802
[54] Shen K, Vignale G and Raimondi R 2014 Microscopic theory of the inverse edelstein effect *Phys. Rev. Lett.* **112** 096601
[55] Mosendz O *et al* 2010 Quantifying spin Hall angles from spin pumping: experiments and theory *Phys. Rev. Lett.* **104** 046601
[56] Bode M *et al* 2007 Chiral magnetic order at surfaces driven by inversion asymmetry *Nature* **447** 190–3
[57] Moriya T 1960 Anisotropic superexchange interaction and weak ferromagnetism *Phys. Rev.* **120** 91–8
[58] Jia C, Onoda S, Nagaosa N and Han J H 2007 Microscopic theory of spin-polarization coupling in multiferroic transition metal oxides *Phys. Rev.* B **76** 144424